Fuel 131 (2014) 17–27

Contents lists available at ScienceDirect

Fuel

journal homepage: www.elsevier.com/locate/fuel

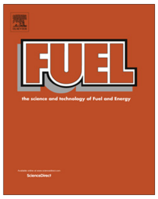

Integrating physicochemical information to follow the transformations of biomass upon torrefaction and low-temperature carbonization

Juliana G. Pohlmann [a,b,*], Eduardo Osório [a], Antônio C.F. Vilela [a], María Antónia Diez [b], Angeles G. Borrego [b]

[a] *Federal University of Rio Grande do Sul (UFRGS), Iron and Steelmaking Laboratory (LASID), P.O. Box 15021, 91501-970 Porto Alegre, RS, Brazil*
[b] *Instituto Nacional del Carbón (INCAR-CSIC), Francisco Pintado Fe 26, 33011 Oviedo, Spain*

HIGHLIGHTS

- Softwood, hardwood and olive stone heated at 250 and 450 °C were characterized.
- Results from bulk chemical and physical techniques and microscopy were integrated.
- Moderate chemical and structural changes occurred at 250 and drastic ones at 450 °C.
- Differences between hardwood and softwood were subtle, but large for olive stone.
- Greater heterogeneity was observed at torrefaction than at carbonization temperatures.

ARTICLE INFO

Article history:
Received 17 February 2014
Received in revised form 16 April 2014
Accepted 18 April 2014
Available online 2 May 2014

Keywords:
Woody biomass
FTIR spectroscopy
Optical reflectance
Spectral fluorescence
Combustion behavior

ABSTRACT

Morphological and structural changes of different types of biomass after torrefaction and low-temperature carbonization processes have been investigated using a variety of characterization techniques comprising Fourier-Transform infrared spectroscopy (FTIR), gas adsorption at different pressures, thermogravimetry, optical and scanning electron microscopy techniques together with chemical analysis. The biomasses selected included softwood chips (pine), hardwood chips (acacia, eucalyptus, forest residues from eucalyptus) and olive stone. Torrefaction led to the enrichment of carbon and a decrease in reactivity, accompanied by a decrease in the hydrogen- and oxygen-bearing functionalities and a slight increase in aromatization. This was physically reflected in cell-wall shrinkage, resulting in a brittle, well-defined vegetal structure with moderate microporosity, in which slight increase in cell-wall reflectance and significant decrease in fluorescence have been produced. Carbonization at 450 °C in turn led to a further loss of oxygen functionalities and a large increase in aromaticity, reflecting the virtual disappearance of hemicellulose and cellulose. This caused a significant increase in optical reflectance, loss of fluorescence and development of both meso- and microporosity generating an isotropic solid with a disordered structure similar to that of industrial charcoal. The microscopy techniques also showed the heterogeneity of the treated samples in terms of reflectance distribution or fluorescence properties, which cannot be assessed by bulk characterization techniques. They indicated a greater heterogeneity in the sample treated at torrefaction temperatures. The different characterization techniques have revealed minor differences between hardwood and softwood behavior, essentially attributed to resinous impregnations in the latter, whereas greater differences were observed between woods and olive stone due to significant differences in their internal and external structure.

© 2014 Elsevier Ltd. All rights reserved.

1. Introduction

Partial substitution of fossil fuels by biomass in industrial processes has become attractive because its utilization could contribute significantly to a reduction in CO_2 from fossil fuels emissions. Nowadays, biomass is considered a neutral C-source because the CO_2 generated by combustion is compensated for by the CO_2 absorbed from the atmosphere during plant growth [1]. Considering biomass as a neutral C-source necessarily requires that forest management is conducted in a sustainable way via a steady and contrasted supply of biomass through energy crops. The partial replacement of fossil fuels by biomass may contribute to protecting the environment in the short-medium term [2]. As regards

---

* Corresponding author at: Federal University of Rio Grande do Sul (UFRGS), Iron and Steelmaking Laboratory (LASID), P.O. Box 15021, 91501-970 Porto Alegre, RS, Brazil. Tel.: +55 51 3308 7074; fax: +55 51 3308 7116.
E-mail address: juliana.pohlmann@ufrgs.br (J.G. Pohlmann).

http://dx.doi.org/10.1016/j.fuel.2014.04.067
0016-2361/© 2014 Elsevier Ltd. All rights reserved.

the two major uses of coal (energy generation and metallurgical coke production), biomass is currently used in relatively small-sized boilers for heating purposes but it is gradually being incorporated into large-scale power generation plants in combination with traditional fuels [3]. Charcoal mainly produced in beehive kilns from eucalyptus wood is also used as an energy source and as chemical reducing agent in mini blast-furnaces in Brazil [4–7]. Recently, the use of charcoal in large metallurgical coke-based blast furnaces with pulverized coal injection [8,9], and as an additive in coal blends for metallurgical coke production are also being explored [9–12].

The partial substitution of biomass for coal is not only attractive because of the environmental benefits, but also because some types of biomass, like wood, have low inorganic matter and impurity contents (e.g. sulfur), which are typical contaminants in many processes [13]. However, some features common to raw biomass such as a high moisture, and a high oxygen content, a low heating value and even its fibrous structure, which makes grinding difficult, are often undesirable in industrial processes. These characteristics make it difficult to handle biomass, and increase the energy consumption which is especially disadvantageous when the biomass has to be ground to a pulverized size [14]. Biomass thermal treatment under an inert atmosphere at mild temperature between 200 and 300 °C (torrefaction) and at moderate temperature between 400 and 500 °C (carbonization) improves its characteristics for use as an energy source in different processes [15–18]. Through heating, biomass undergoes chemical, physical and structural transformations whose magnitude depends on the final temperature of the treatment [15,16,19]. The main bulk transformations upon torrefaction are a reduction in hygroscopicity [20–23] and an improvement in grindability [23–26] and energy density [20,27], whereas carbonization leads to greater carbon enrichment, which is preferred for energy purposes [28,29], despite the lower solid yield. Optimum torrefaction conditions have been established for around 30% mass loss, which gave a 20% increase of higher heating value [16].

Among the techniques used for characterization of thermally treated biomass, thermogravimetric analyses have shown little variation in the combustion characteristics of biomass treated at below 300 °C [24,30], and also similar distributions of pore size determined by N_2 adsorption for torrefied and raw biomasses [23]. Structural models based on spectroscopic techniques [23,31] of carbonized biomass suggest a rather aromatic highly conjugated structure with significant amounts of oxygen heteroatoms, which correspond to solids with values of specific surface area of few hundreds depending on the treatment temperature [31]. Both treatment temperature and feedstock have shown to have an impact in the characteristics of the biochars [30,31].

In the present work, the results of chemical, spectroscopic, physical adsorption and microscopic techniques have been integrated to study the transformations occurring in biomasses of different characteristics (softwood and hardwood chips and olive stones) during the thermal treatments of different severity. The main contribution is the combination of results from bulk techniques providing information of the whole sample and quantitative microscopy, able to describe the heterogeneity of the sample.

2. Material and methods

Four types of biomass were selected: softwood chips of *Pinus illiotis* (Pin), hardwood chips of *Acacia mangium* (Aca) and *Eucaliptus saligna* (Euc), the residual biomass from an unselected collection of *Eucaliptus saligna* (Rec), and olive stone from *Olive europaea* (Ols). The wood chips were sieved to 19 mm and the olive stone was maintained at its commercialization size of below 5 mm. Thermal treatments were conducted in a vertical furnace at atmospheric pressure, under a nitrogen flow of 50 mL min^{-1}, at a heating rate of 5 °C min^{-1} up to the target temperature with a holding time of 30 min. Samples were dried at 50 °C before thermal treatment and the amount of sample used in each test was 40 g. Two different target temperatures were selected: 250 °C to generate torrefied biomass and 450 °C to generate charcoal. The suffixes "to" and "ca" identify these samples, respectively.

The samples were subjected to proximate and ultimate analyses as well as tests for total sulfur content and higher heating value (HHV) according to the ISO 17246:2010, ISO 29541:2010, ISO 19579:2006 and ISO 1928:2009 standards, respectively.

The pore surface area of the thermally treated biomasses was determined by gas adsorption isotherms using N_2 at −196 °C and CO_2 at 0 °C as adsorptives with a Micromeritics ASAP 2020 equipment. The samples were outgassed while heated at 5 °C min^{-1} in two steps: (1) up to 90 °C with 1 h holding time; (2) up to 150 °C for the torrefied biomasses and up to 350 °C for the carbonized biomasses, with a holding time of 4 h. The temperatures used for outgassing are well below the temperatures used for the thermal treatment of biomasses and were not expected to modify their porous structure. The Brunauer–Emmett–Teller (BET) theory was applied to the N_2 adsorption data in the interval of relative pressure (P/P_0) 0.05–0.3 to determine the mesopore surface area [32]. CO_2 adsorption isotherms were performed up to a pressure of 0.035 torr to evaluate the micropore surface area. The Dubinin–Radushkevich (D–R) equation [33] was applied to all adsorption data (up to P/P_0 of 0.035), and a value of 0.17 was used for the molecular cross-sectional area.

Fourier-Transform infrared (FTIR) spectra were collected in a Nicolet IR 8700 spectrometer fitted with a mercury-cadmium telluride detector (MCT-A) operating at sub-ambient temperature and a Smart Collector diffuse reflectance (DRIFT) accessory. Spectra were obtained by co-adding 100 scans at a resolution of 4 cm^{-1}. Several FTIR indices derived from the maximum intensity (I) of selected absorption bands were used to assess the changes in the chemical structure of the biomass.

Morphological variations in the biomass upon heating were assessed by using a JEOL JSM 6060 microscope (SEM) and both the physical transformations and morphological changes were determined using a reflected light DMP 4500 optical microscope (OM) equipped with 50× oil immersion objectives. Cell-walls reflectance was measured in the torrefied and carbonized samples following the ISO 7404-5:2009 standard for vitrinite reflectance measurements in coal. Fluorescence spectra of the raw and torrefied biomasses were measured using ultraviolet light excitation and corrected using the spectrum of a quartz-iodine lamp according to the procedure described by Baranger et al. [34]. For each component around 20 spectra were averaged. The parameters used for comparing the different spectra were $\lambda_{\max}$ (wavelength of maximum fluorescence intensity) and the red/green quotient ($Q_{R/G}$ = intensity at 650 nm/intensity at 500 nm).

Combustion at programmed temperature was measured in a TG 7 Perkin–Elmer thermoanalyzer. Approximately 13 mg of sample ground to <212 μm were heated under an air flow of 50 mL min^{-1} from 50 °C to 900 °C at a heating rate of 20 °C min^{-1}. From the first derivative of the weight loss curve (DTG), several combustion parameters were derived: initial burning (Ti), maximum (Tp) and final or burnout (Tf) temperatures, defined as the temperature at which reactivity is 1/5 of the maximum [35], peak temperature, and temperature at which weight loss have ceased, respectively. The maximum reaction rate (ash-free basis) was calculated as $R_{\max} = -1/w_0\,(dw/dt)$, where w_0 is the initial weight of the sample.

3. Results and discussion

3.1. Raw biomasses characteristics

Raw biomasses were characterized by high volatile matter and oxygen contents as well as low ash, carbon, nitrogen and sulfur contents [36]. As can be seen from Table 1 the HHV of the raw biomasses used in this study was about 20 MJ kg^{-1}. Only minor differences in the chemical composition were observed between the raw biomasses as regards the volatile matter (82.1–83.9%), C (48.9–51.6%) and S (0.01–0.09%) contents (Table 1). The highest ash content corresponding to the eucalyptus residues (Rec) was associated to its more heterogeneous composition comprising not only wood but also leaves and other plant components.

The FTIR spectra of the raw biomasses are shown in Fig. 1 and a more detailed explanation of the band assignments is provided in Table 2. All the spectra were characterized by features common to biomass: a broad band due to the stretching vibration of hydrogen bonded O—H around 3400 cm^{-1} (νO—H); the typical C—H stretching vibrations between 2980 and 2750 cm^{-1} assigned to aliphatic groups (νCH$_{al}$); a prominent band centered at 1735 cm^{-1} due to C═O stretching in non-conjugated and conjugated systems (carbonyl/carboxyl groups) whose intensity is used to estimate the lignin/carbohydrate relative abundances in woody biomass [38]; a band at nearly 1650 cm^{-1} attributed to O—H absorbed in conjugated C—O bonds [45], which was a distinct feature of hardwood and olive stone, appearing as a broad band joined to the aromatic νC═C band in the softwood spectrum; the typical carbohydrate bands of cellulose and hemicelluloses at 1375 cm^{-1} (C—H deformation vibration), at 1158 cm^{-1} (C—O—C vibrations), 1048 cm^{-1} (C—O stretch vibrations) and 898 cm^{-1} (C—H deformation in polysaccharides); νC═C bands characteristic of lignin at 1596 and 1506 cm^{-1}, whose relative intensity was dependent on the type of biomass; the absorption bands attributed to lignin in the region 1000–1400 cm^{-1}, which were only slightly different in softwood and hardwood. Additionally, the Pine softwood spectrum showed two distinct bands at 1271 and 1232 cm^{-1} attributed to the guaiacyl-type lignin [37], whereas hardwood lignin presented a single band at around 1250 cm^{-1}, which refers to the syringyl nuclei [38]. The olive stone spectrum showed a single band in this region shifted to higher wavenumber than the lignin hardwood band (1264 compared to 1250 cm^{-1}). The aliphatic C—H deformation vibrations (δCH$_{al}$) corresponding to polysaccharides were also present in all the spectra (bands at 1456 and 1426 cm^{-1}, also assignable to the δCH$_{al}$ of lignin; and the band at 1375 cm^{-1}).

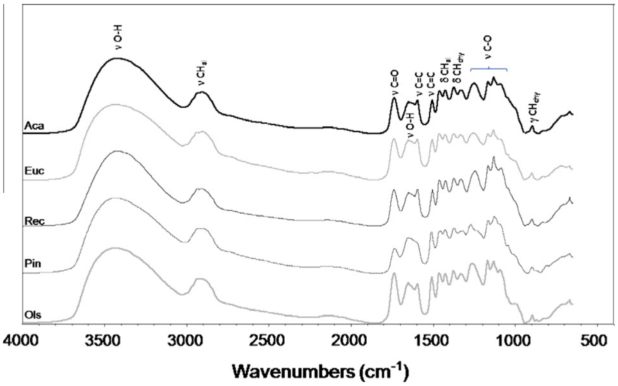

Fig. 1. FTIR spectra of raw biomasses.

Several FTIR indices as defined in Table 3 can be used to follow the wood decay [38]. The I_{ar}/I_{al} ratio, which is widely used to estimate aromaticity [46,47], showed high values for three samples Rec, Pin and Ols. Aromaticity in biomass is related to lignin macromolecule built from polyphenyl propane units, mainly guaiacyl propane (G) and syringyl propane (S), which are bonded to each other by several linkages. Thus, differences in the C═C environment are reflected in the $I_{C{=}Clig}$ index. While the hardwoods had a ratio near to unity, the softwood and Ols spectra showed a high amount of aromatic C═C bonds absorbing close to 1506 cm^{-1}, allowing the hardwoods to be distinguished from the softwoods and reflecting a sort of lignin maturity as the 1506 cm^{-1} band tended to disappear in the carbonized samples (Table 4).

As regards the carbohydrate (CHY) abundances in the raw biomasses, three indices were used: $I_{C{=}C}/I_{C{=}O}$, I_{LIG}/I_{CHY} and $I_{LIG}/I_{CHY}2$. The $I_{C{=}C}/I_{C{=}O}$ ratio is probably not only an estimation of lignin to carbohydrate abundances in the raw samples, but also an indication of the relative abundances of oxygen functionalities to aromatic rings in the thermally treated samples. The I_{LIG}/I_{CHY} ratio was greater than unity for Pin (softwood) sample (Table 4), indicating higher lignin content in the softwoods [48]. The $I_{LIG}/I_{CHY}2$ ratio was lower in Pin than one would expect from the high values of the I_{LIG}/I_{CHY} ratios and $I_{C{=}C}/I_{C{=}O}$ due to the large differences in intensity of the two lignin νC═C bands.

Table 1
Chemical analyses of raw and thermally treated biomasses expressed on a dry basis.

Biomass	Proximate analysis (wt%)			Ultimate analysis (wt%)				Total sulfur (wt%)	HHV (MJ kg^{-1})
	Ash	VM	FC	C	H	N	O$_{dif}$	S$_{tot}$	
Raw samples									
Aca	1.12	83.94	14.94	48.93	6.06	0.43	43.44	0.02	19.5
Euc	0.79	82.55	16.66	49.79	6.02	0.37	42.95	0.08	19.6
Rec	1.26	80.98	17.76	49.66	6.09	0.54	42.39	0.06	19.5
Pin	0.70	82.10	17.20	51.10	6.14	0.41	41.56	0.09	20.0
Ols	0.37	82.41	17.22	51.62	5.97	0.25	41.78	0.01	20.5
Torrefied samples									
Aca-to	2.47	70.06	27.47	54.95	5.47	0.60	36.47	0.04	21.9
Euc-to	0.89	73.77	25.34	55.41	5.73	0.45	37.48	0.04	22.7
Rec-to	2.03	69.86	28.11	57.04	5.64	0.67	34.58	0.04	22.5
Pin-to	0.86	73.29	25.85	57.11	5.76	0.48	35.77	0.02	21.8
Ols-to	0.37	77.10	22.53	55.04	5.80	0.17	38.60	0.02	22.0
Carbonized samples									
Aca-ca	5.03	14.92	80.05	83.58	3.09	0.84	7.45	0.01	31.7
Euc-ca	2.44	16.52	81.04	85.02	3.16	0.57	8.80	0.01	32.4
Rec-ca	3.61	15.66	80.73	85.31	3.20	0.89	6.97	0.02	32.1
Pin-ca	1.72	25.72	72.56	78.24	3.52	0.60	15.92	<0.01	30.7
Ols-ca	1.28	15.98	82.74	86.28	3.32	0.46	8.65	0.01	33.3

Table 2
Main band assignments of the FTIR spectra of the raw, torrefied and carbonized biomasses.

Wavenumber (cm^{-1})	Band assignment	References
3400	Hydrogen-bonded O—H	[12,37–40]
3050	C—H stretching of aromatic rings in carbonized samples (νCH_{ar})	[41,42]
2800–2900	C—H stretching of methyl and methylene groups (νCH_{al})	[12,39,40,42,43]
1735–1739	C=O stretching modes (νC=O) attributed to oxygenated functionalities in non-conjugated and conjugated systems (carbonyl/carboxyl groups)	[12,38–40]
1647–1653	Absorbed O—H and conjugated C—O	[38,45]
1596 and 1506–1510	Aromatic skeletal vibrations in lignin (νC=C). Shift to higher wavenumbers upon heating	[12,38,39,43,44,46]
1456–1465 and 1426–1428	C—H deformations in lignin and carbohydrates (δCH_{al})	[12,37,38,44]
1376	C—H deformation in cellulose and hemicellulose (δCH_{chy})	[38,44]
1320–1333	C—H vibration in cellulose and C—O vibration in syringyl derivatives	[38,44]
1271 (Only in softwood)	Attributed to a mode associated with the guaiacyl ring, C—O stretching in lignin and C—O linkage in guaiacyl aromatic methoxyl groups	[37,38,43]
1232 (Only in softwood)	Attributed to a combination of a deformation of the syringyl ring and a deformation of cellulose	[37,43]
1246–1257 (Only in hardwoods)	Syringyl ring	[37,38,44]
1167–1170	Antisymmetrical bridge oxygen stretching (νC—O—C)	[38]
1128–1134 and 1086–1093	C—O stretching modes (νC—O)	[38,44]
899	C—H deformation in cellulose (γCH_{chy})	[37,38,44]
700–900	Three bands corresponding to out-of-plane deformation 1–4 adjacent C—H bonds in aromatic rings (γCH_{ar})	[39–41,43,47]

Table 3
Infrared Indices used in this paper and their significance.

FTIR index	Definition	Absorption bands	Significance
I_{LIG}/I_{CHY}	I_{1506}/I_{1736}	νC=C 1506 cm^{-1} νC=O 1735 cm^{-1}	Relative abundance of lignin and carbohydrates
$I_{C=Clig}$	I_{1596}/I_{1506}	νC=C 1596 and 1506 cm^{-1}	Lignin maturity
$I_{LIG}/I_{CHY}2$	I_{1596}/I_{1646}	νC=C 1596 cm^{-1} νC—O and C—O 1646 cm^{-1}	Decay of wood involving lignin C=C bands and O—H absorbed in conjugated C—O bonds
$I_{C=C}/I_{C=O}$	I_{1596}/I_{1736} (raw) I_{1608}/I_{1716} (to) I_{1608}/I_{1696} (ca)	νC=C 1596 or 1608 cm^{-1} νC=O 1736 or 1716 or 1696 cm^{-1}	Relative abundance of oxygen functionalities
I_{ar}/I_{al}	I_{1596}/I_{2936}	νC=C (1596–1608 cm^{-1}) νCH_{al} (2936 cm^{-1})	Aromaticity

Microscopic observations by SEM and OM revealed very similar structures in the Euc and Rec samples (Fig. 2). The woody biomasses showed large and elongated particles with a fibrous appearance, and without any significant porosity (Fig. 2a and d). Under a reflected light optical microscope, the samples were translucent in white light (Fig. 2b and e) showing occasionally reddish internal reflections. They exhibited an intense green fluorescence under blue–violet[1] light (Fig. 2c and f). The eucalyptus residue consisted of woody material as the major component and a variety of other plant components. Among the non-woody components Fig. 2e and f shows the presence of a cuticle attached to the parenchyma tissue of a leaf that exhibited a more orange fluorescence (Rec-cut). Its spectrum had a high intensity in the red region (Fig. 3a). The highest intensity fluorescence spectra were those of acacia, intermediate and similar intensities could be observed for the Euc, Rec and Pin spectra and the lowest intensity spectra correspond to those of Olive stone (Fig. 3a). Both the Aca and Euc woody tissues exhibited certain heterogeneity in their fluorescence properties, with a few tissues exhibiting a yellowish color and a shoulder in the blue region of their spectra, like most of the woody material in the samples (Fig. 3b and c). The shift to longer wavelengths of Euc-2 and Aca-2 spectral maxima compared to those representing the majority of the sample (540 nm vs 440 nm) may be attributed to oxidation or alteration of the component, as occurs in coal [49]. The parameters derived from the spectra are shown in Table 5. Both λ_{max} and $Q_{R/G}$ were similar in the case of lignocellulose tissues with spectral maxima at 440 nm and a very low $Q_{R/G}$ value (0.1 for the Aca, Rec and Ols samples and 0.2 for Euc and Pin). The differences in the fluorescence spectra of the cuticles in the Rec sample reflected different chemical compositions, indicating lipidic substances [50] with an intense reddish fluorescence (λ_{max} = 675 nm; Fig. 3a).

Table 4
FTIR indices related to lignin and carbohydrates absorption bands in raw, torrefied and carbonized biomasses.

Samples	I_{LIG}/I_{CHY}	$I_{C=Clig}$	$I_{LIG}/I_{CHY}2$	$I_{C=C}/I_{C=O}$	I_{ar}/I_{al}
Raw					
Aca	0.91	1.00	1.06	0.91	0.88
Euc	0.95	1.02	1.03	0.97	0.95
Rec	0.97	1.04	1.12	1.01	1.17
Pin	1.66	0.77	0.92	1.28	1.25
Ols	0.89	0.85	0.99	0.76	1.32
Torrefied					
Aca-to	1.26	0.99	1.34	1.09	1.02
Euc-to	1.44	0.92	1.40	1.15	1.32
Rec-to	1.23	1.06	1.39	1.12	1.18
Pin-to	1.65	0.75	1.39	1.12	1.43
Ols-to	0.91	1.15	1.15	0.77	1.33
Carbonized					
Aca-ca	–	–	–	2.11	11.13
Euc-ca	–	–	–	2.12	12.18
Rec-ca	–	–	–	2.28	13.26
Pin-ca	–	–	–	2.02	9.10
Ols-ca	–	–	–	2.21	8.45

---

[1] For interpretation of color in Figs. 2, 3, 6, and 7, the reader is referred to the web version of this article.

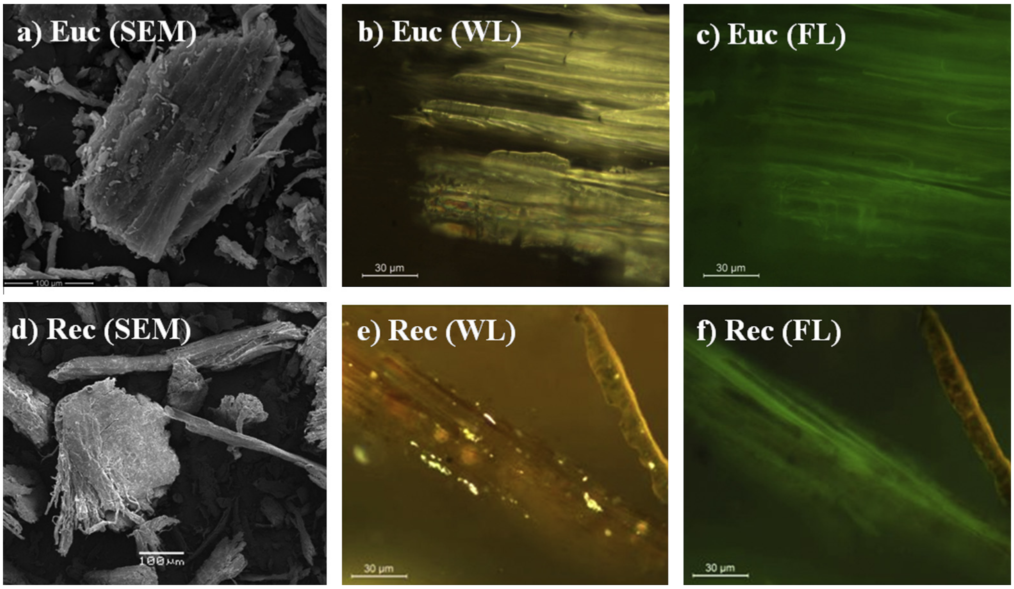

Fig. 2. Appearance of raw biomasses under the scanning electron microscope (a and d) and the optical microscope (b, c and e, f). WL = white light, FL = Fluorescent light. Optical microscope images were taken under incident light and oil immersion objectives.

3.2. Combustibility of the biomasses

The DTG curves of raw biomasses obtained in air are conform to the typical combustion profiles with three distinct peaks, each corresponding to a weight loss step (Fig. 4). Those of the softwood (Pin), hardwood (Euc) and Olive stone (Ols) are shown as an example. The first peak at nearly 100 °C corresponded to the moisture loss. The second peak from 200 to 400 °C corresponded to the overlapping of the burning modes of hemicellulose and cellulose, the former known to burn at slightly lower temperatures than the latter [51,52]. The hardwood samples (Aca, Euc and Rec) exhibited the shoulder related to the decomposition/combustion of hemicellulose (see Euc in Fig. 4a), while the maximum reactivity corresponded to the combustion of cellulose [51,52]. Pine did not show a well-defined hemicellulose shoulder (Fig. 4b), probably due to the lower hemicellulose content in softwoods [48], whereas Olive stone exhibited two maxima of similar intensity (Fig. 4c and Table 6) in this region, having the lowest values of maximum reactivity. The composition of the Olive stone essentially consists of hemicellulose, cellulose and lignin, with hemicellulose and cellulose contents being closer than in the wood chips, and cellulose being significantly lower than that of softwood [48,53]. The third peak above 400 °C, which is attributed to the combustion of lignin and the combustion of the char formed by resolidification of the carbonaceous material [40,51], had the widest burning interval. Pin sample showed the highest combustion temperatures of all the raw samples indicating a high thermal stability (Table 6). This is attributed to its higher lignin content compared to hardwood [52].

3.3. Transformations during the thermal treatment

The main transformations occurring upon torrefaction and carbonization were associated with an increase in the amount of ash – although the amount of ash was still low in the carbonized sample – a decrease in the volatile matter, and H and S contents and an increase in the C and N contents (Table 1). A high thermal stability of the N-functionalities, which were retained in the carbonaceous solid, is derived from elemental analysis, whereas most of the S was released as volatiles. The changes in chemical composition were reflected in the HHV, which increased up to values typical of a subbituminous coal in the case of the torrefied samples and to a high volatile bituminous A rank in the case of the carbonized samples, according to the ASTM coal rank classification (ASTM D388).

Generally, the samples which were heated at the same temperature showed a similar chemical composition, regardless of the type of wood. The torrefied samples, which experienced the lowest temperature treatment, still retained high amounts of volatile matter and oxygen and have low ash and carbon contents (Table 1), the exception being the carbonized pine, which showed a higher volatile matter and H content and a lower C content than the other carbonized biomasses. This difference could be due to the effect of resinous H-rich impregnations occurring in conifers [54].

The main features characterizing the changes in FTIR spectra of the biomasses upon pyrolysis can be seen in Fig. 5 and summarized as follows: a significant decrease in hydroxyl (νO—H) and aliphatic bonds (νCH_{al}), together with the formation of condensed aromatic rings, evidenced by the presence of a νCH_{ar} stretching band at 3050 cm^{-1}, is observed in the carbonized samples. The oxygen functionalities (at 1700 cm^{-1} and 1400–1000 cm^{-1}) showed a slight decrease from the raw to the corresponding torrefied sample, essentially due to the loss of hemicellulose at the mild torrefaction temperature. A further increase in temperature during carbonization resulted in the almost complete loss of oxygen-bearing functionalities (Fig. 5). The aromatic C═C bands centered at 1596 and 1506 cm^{-1} in the raw biomasses were slightly shifted to a higher wavenumber (1606 and 1512 cm^{-1}, respectively) in the torrefied spectra and only the band at 1606 cm^{-1} was present in the carbonized spectra. These structural changes can be clearly associated to the loss of oxygen-functionalities and aromatic condensation. The lignin/carbohydrate ratios (I_{LIG}/I_{CHY}, $I_{LIG}/I_{CHY}2$) increased due to torrefaction (Table 4), indicating that in all the biomasses most of the hemicellulose had decomposed leading to a concentration of the lignin. The softwood sample continued to have the highest I_{LIG}/I_{CHY} value, although the $I_{LIG}/I_{CHY}2$ ratios were similar for softwood and hardwoods, and both I_{LIG}/I_{CHY} and I_{LIG}/I_{CHY} ratios had the lowest value for the Ols sample compared to the woody material. A slight increase in aromatization and a decrease in oxygen-bearing functionalities upon torrefaction was observed

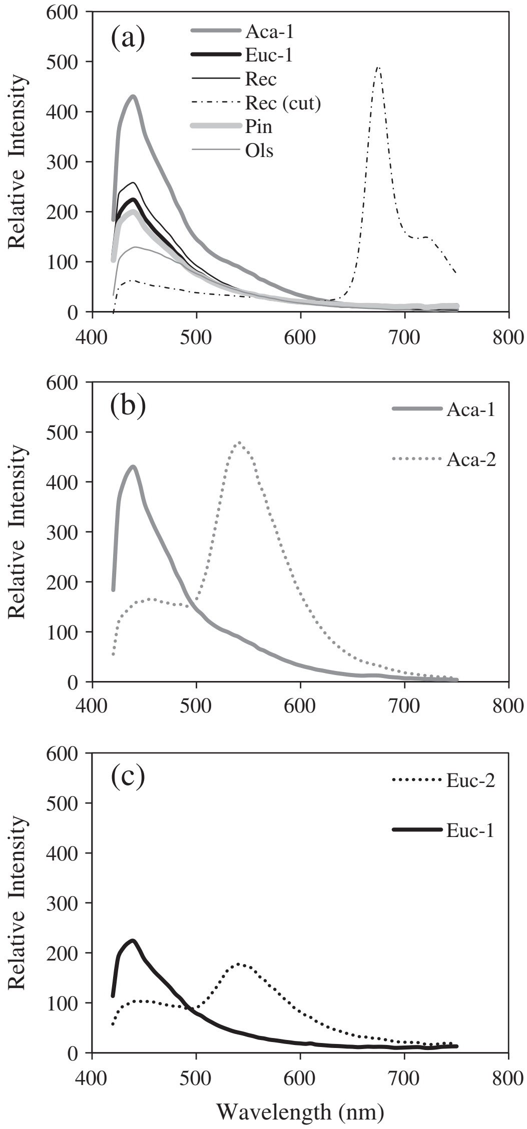

Fig. 3. Fluorescence spectra of raw biomasses. (a) Lignocellulosic tissues and cutinite in sample Rec, (b) variability of lignocellulosic tissues in Aca sample and (c) variability of lignocellulosic tissues in Euc sample.

Table 5
Petrographic parameters of the samples: Rr = random reflectance, CV_{Rr} = coefficient of variation of reflectance readings calculated as the quotient between the standard deviation and the mean, λ_{max} = spectral maximum and $Q_{R/G}$ = red/green quotient in the fluorescence spectra.

Sample	Rr (%)	CV_{Rr}	λ_{max} (nm)	$Q_{R/G}$
Raw samples				
Aca-1	–	–	440	0.1
Aca-2	–	–	540	0.3
Euc-1	–	–	440	0.2
Euc-2	–	–	540	0.4
Rec	–	–	440	0.1
Rec-cut	–	–	675	1.7
Pin	–	–	440	0.2
Ols	–	–	440	0.1
Torrefied samples				
Aca-to	0.18	0.50	600	1.0
Euc-to	0.12	0.50	630	1.2
Rec-to	0.14	0.50	590	1.1
Pin-to	0.10	0.60	575	0.8
Ols-to	0.10	0.40		
Blue (frequency: 9%)	–	–	440	0.3
Yellow (frequency: 22%)	–	–	555	0.7
Orange pale (frequency: 24%)	–	–	585	1.0
Orange dark (frequency: 24%)	–	–	585	1.5
Brown (frequency: 22%)	–	–	620	1.7
Carbonized samples				
Aca-ca	1.88	0.16	–	–
Euc-ca	1.95	0.14	–	–
Rec-ca	2.03	0.14	–	–
Pin-ca	1.75	0.15	–	–
Ols-ca	1.96	0.09	–	–

in the I_{ar}/I_{al} and $I_{C=C}/I_{C=O}$ indices, respectively (Table 4). The drastic increase in both indices reflected the virtual disappearance of hemicellulose and cellulose in the carbonized samples (Table 4). The increase in aromatic structures was also reflected in the presence of three well-resolved bands in the 700–900 cm^{-1} region corresponding to the out-of-plane vibration of aromatic C—H bonds (γCH$_{ar}$) with an isolated H and 2–4 adjacent hydrogens in the aromatic rings [46]. These bands are typically present in medium to high rank coal FTIR spectra [39,41,47]. The values of the $I_{C=C}/I_{C=O}$ ratio were rather similar for the carbonized samples, whereas the I_{ar}/I_{al} ratios indicated a lower aromaticity for Ols-ca and the Pin-ca (Table 4). The lower aromaticity values recorded for softwood could be related to its higher volatile matter content (Table 1), whereas in the case of Ols-ca, with similar volatile matter content to hardwood, its lower aromaticity may be related to its significantly distinct structure.

Table 7 shows the pore volume and specific surface areas corresponding to the meso- (S_{BET}) and micropores (S_{D-R}) of the biomasses thermally treated at different temperatures. The S_{BET} values of the torrefied biomasses were negligible, according to values <1–8 m^2 g^{-1} reported previously [23,30,55]. The structure of low temperature thermally treated biomass may shrink at the low temperatures at which the N_2 adsorption isotherms are carried out, resulting in unrealistic low values [56]. The CO_2 at 0 °C diffuses easily and may partially overcome this difficulty [57]. Values between 50 and 92 m^2 g^{-1} were reached by the S_{D-R} of micropores. Accordingly, the pore volumes measured by means of N_2 adsorption ranged between 0.002 and 0.007 cm^3 g^{-1}, whereas those measured by CO_2 adsorption ranged between 0.011 and 0.019 cm^3 g^{-1} (Table 7) indicating that most of the porosity is below 7 Å and that it is a tortuous and strangulated porosity [57]. The carbonization process generated a carbonaceous solid with relatively high S_{BET} and S_{D-R} values resulting from a significant release of volatiles and the resolidification of the carbonaceous material. The volumes of the N_2 and CO_2 pores were similar, but the N_2-measured volumes slightly exceed those of CO_2-measured pores in the woody biomasses, indicating a significant increase in the size of the pores, the exception being the Ols-ca sample, whose S_{BET} (24.1 m^2 g^{-1}) and N_2 pore volume (0.023 cm^3 g^{-1}) were much lower than those of the other carbonized biomasses (Table 7). The micropore surface area and pore volume of the Ols-ca sample, however, were very similar to the other carbonized samples. The microporous structure is generally attributed to the arrangement of the carbonaceous skeleton – the interlayer spacing and the disorientation of the layers, and this structure is similar in all the carbonized biomasses. The mesoporous structure is more related to the spaces left by the release of volatiles [58]. The combination of S_{BET} and S_{D-R} results in Ols-ca sample indicated a much smaller pore size for this sample than for the woody biomasses likely due to the thicker walls of olive stone, which might prevent an easy diffusion of volatiles that would enlarge and connect the porosity.

The biomasses maintained upon heating their characteristic cellular structure formed by cell-walls and empty channels, the main transformation being cell-wall shrinkage, which resulted in thinner and multilayered walls (see image for Euc-to in Fig. 6a). This shrinkage was probably caused by the partial loss of hemicellulose, which decomposes under an inert atmosphere at temperatures

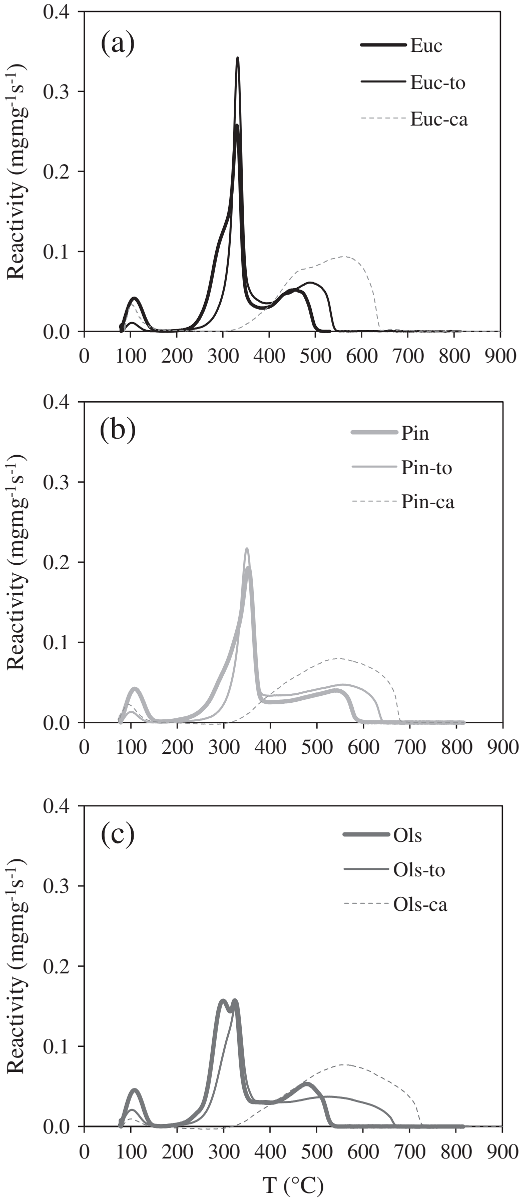

Fig. 4. Burning profiles recorded at increasing temperature in a thermobalance for raw, torrefied and carbonized eucalyptus (a), pinus (b) and olive stone (c).

Table 6
Characteristic temperatures and maximum reaction rates extracted from the combustion profiles of raw, torrefied and carbonized biomasses. T_{max} (1) and R_{max} (1) correspond to the Temperature of maximum reactivity (T_{max}) and maximum reactivity (R_{max}) of the hemicellulose/cellulose peak and T_{max} (2) and R_{max} (2) refer to the corresponding values of the lignin peak.

Sample	Ti 1/5R_{max}	T_{max} (1)	T_{max} (2)	Tf	R_{max} (1)	R_{max} (2)
	(°C)				(mg mg^{-1} s^{-1})	
Raw samples						
Aca	272	338	488	534	0.209	0.038
Euc	271	330	457	515	0.258	0.052
Rec	265	325	455	510	0.224	0.054
Pin	279	352	538	600	0.193	0.040
Ols	256	299/324	476	539	0.157/0.157	0.053
Torrefied samples						
Aca-to	305	335	500	567	0.270	0.059
Euc-to	307	332	488	551	0.343	0.061
Rec-to	294	320	438	577	0.286	0.068
Pin-to	313	350	556	644	0.217	0.047
Ols-to	272	327	525	670	0.157	0.037
Carbonized samples						
Aca-ca	364	547	–	6905	–	0.077
Euc-ca	374	560	–	642	–	0.099
Rec-ca	345	505	–	654	–	0.078
Pin-ca	362	546	–	680	–	0.080
Ols-ca	366	559	–	757	–	0.077

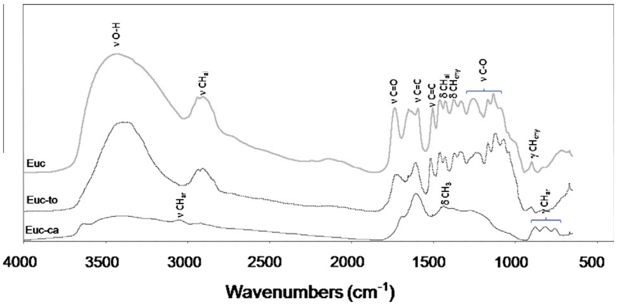

Fig. 5. FTIR spectra of raw, torrefied and carbonized eucalyptus.

below 315 °C [40]. The optical microscopic appearance allowed the distinction of a darker internal and a lighter external part within the walls as illustrated for Euc-to in Fig. 6b. Due to the thinness of the cell-wall the reflectance of the darker and lighter parts could not be separately measured and therefore the reflectance values given in Table 5 reflect an average value for the two areas (dark and light). In addition the image of Fig. 6b corresponded to the most severely transformed material within the sample, whereas many particles still remained translucent with reddish internal reflections. The cell-walls of the Ols-to were thicker than those of the wood chips (Fig. 6d). The increase in reflectance from virtually 0% corresponding to translucent material in the raw biomasses to values between 0.10% and 0.18% in the torrefied biomasses is consistent with the C-enrichment observed in the elemental analysis (Table 1) and a slight increase in aromaticity revealed by FTIR spectroscopy (Table 4). This transformation was common to all the woody chips, resulting in an appearance similar to that of textinite in peat and brown coal [59]. The standard deviations of the reflectance measurements were relatively large for the mean value indicating a large heterogeneity in the samples. The coefficient of variation (CV_{Rr}) calculated as the quotient between the standard deviation and the mean allow a direct comparison of the scatter in the populations regardless the actual value of the mean. The coefficients of variation also confirmed the significant scatter of the reflectance readings, the highest CV_{Rr} been achieved for the softwood and the lowest for the olive stone (Table 5). Under fluorescent light, the cell walls of torrefied biomasses exhibited orange fluorescence (Fig. 6c), which was weaker for the material appearing more opaque under white light. The fluorescence spectra of torrefied biomasses were less intense and noisier than those of the raw biomasses (Figs. 3a and 7a) and were shifted to higher wavelengths (Table 5). The variability of fluorescence properties within the torrefied samples was greater than that of raw biomasses. The greatest heterogeneity was observed in the torrefied olive stone, in which at least five different-colored particles could be detected (blue, yellow, two shades of orange and brown), whose corresponding spectra are shown in Fig. 7b. The spectral parameters of the various populations (Table 5) showed a clear increase in λ_{max} and $Q_{R/G}$ from the values of the virtually untransformed material (λ_{max} = 440 nm, $Q_{R/G}$ = 0.3) to those of the least fluorescing material with brownish color (λ_{max} = 620 nm, $Q_{R/G}$ = 1.7). The variability of Ols-to particles is shown in Fig. 6e and f. Quantification of the amounts of different fluorescing types in the Ols-to sample showed that the blue, nearly untransformed particles were the least common, whereas the other types were present in amounts close to 20% (Table 5). Olive stone, which had the thickest cell-walls, appeared to be the most sensitive to the variation in temperature in the oven. The least fluorescing particles were likely those heated to higher temperatures for longer times (closest to the oven walls) and the most fluorescing ones were the particles closest to the center of the oven, having remained for a shorter time at the targeted temperature. These differences due to mode of heating should have affected all the samples, but woody structures showed smaller differences in fluorescence properties. Either the thicker walls or the smaller particle size of olive stone compared to the woody samples may had affected the heat transmission and could have been responsible for the different behaviors observed. Compared to hardwood, torrefied pine had the highest intensity spectra shifted to lower wavelengths (Fig. 7a; Table 5), consistent with the lower reflectance values (Table 5) among the woody biomasses.

Table 7
Pore volume and specific surface areas corresponding to the meso- (S_{BET}) and micropores (S_{D-R}) of the biomasses thermally treated at different temperatures.

Samples	S_{BET} ($m^2\ g^{-1}$)	S_{D-R} ($m^2\ g^{-1}$)	Pore vol N_2 ($cm^3\ g^{-1}$)	Pore vol CO_2 ($cm^3\ g^{-1}$)
Torrefied				
Aca-to	0.1	49.9	0.002	0.011
Euc-to	3.1	82.3	0.006	0.016
Rec-to	4.5	91.7	0.007	0.019
Pin-to	4.3	84.7	0.006	0.017
Ols-to	0.4	77.9	0.003	0.015
Carbonized				
Aca-ca	234.7	343.8	0.110	0.089
Euc-ca	220.6	370.4	0.128	0.091
Rec-ca	167.0	298.5	0.104	0.078
Pin-ca	192.3	361.1	0.096	0.088
Ols-ca	24.1	333.9	0.023	0.073

The carbonized samples had reflectances ranging from 1.75% to 2.03% (Table 5) and had completely loss fluorescence. The increase in reflectance from torrefied to carbonized samples was large, generating a material very similar to charcoal under both the optical and the SEM microscopes (Fig. 8). The optical microscope revealed an isotropic optical texture, consistent with the homogeneous walls observed by SEM, without any sign of the multilayered structure which was evident at lower heating temperatures (Fig. 8). The images of Fig. 8 show not only the presence of channels in the cell structure but also the existence of small devolatilization pores within the walls. The cell openings in the char structure represent a way out for volatile products during the pyrolysis (Fig. 8a and c). However, the formation of bubbles can be observed in the zoom of

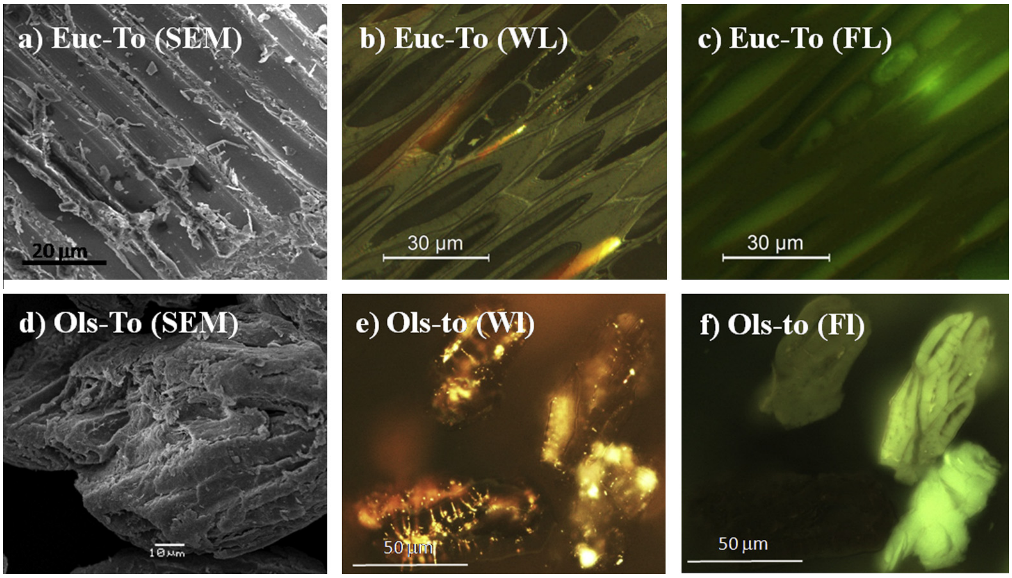

Fig. 6. Appearance of torrefied biomasses under the scanning electron microscope (a and d) and the optical microscope (b, c and e, f). WL = white light, FL = Fluorescent light. Optical microscope images were taken under incident light and oil immersion objectives.

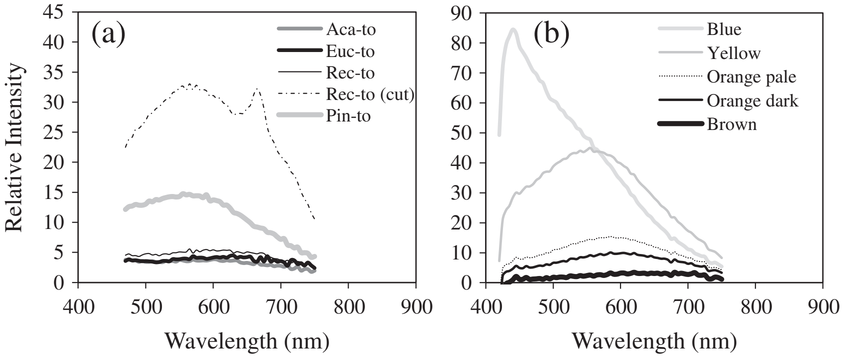

Fig. 7. Fluorescence spectra of torrefied biomasses. (a) Torrefied samples and (b) variability within Ols-to particles.

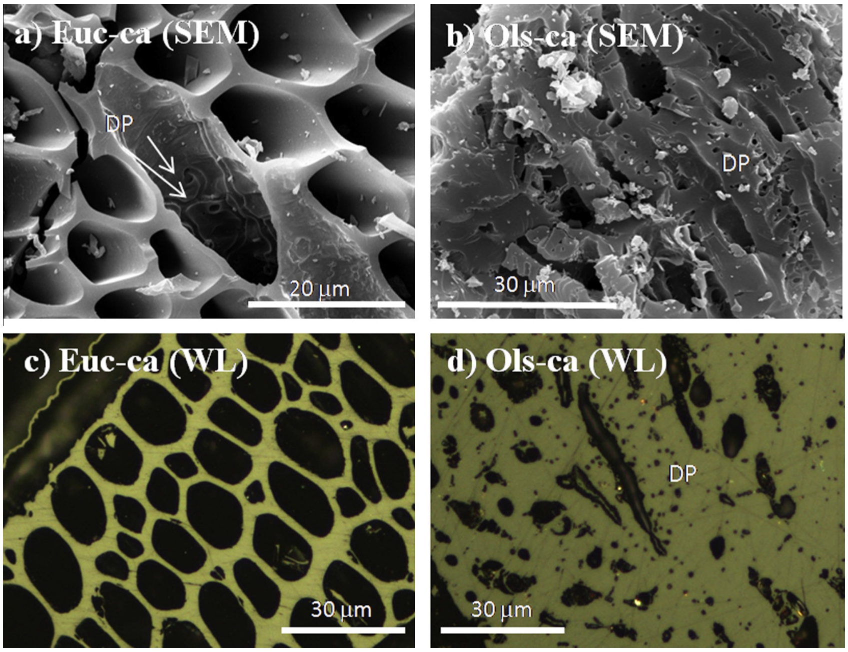

Fig. 8. Appearance of carbonized biomasses under the scanning electron microscope (a and c) and the optical microscope (b and d). WL = white light, FL = Fluorescent light, DP = devolatilization pore. Optical microscope images were taken under incident light and oil immersion objectives.

the surface (Fig. 8a). This is ascribed to the release of volatiles from the internal zones of the particle while the solid material is softening and melting [60]. These bubbles are small and seem to be originated from very small holes in the surface of the material. The structure of Ols-ca under incident white light was more massive and compact and showed a structural porosity that is often difficult to distinguish from the devolatilization pores (Fig. 8b and d).

The isotropic optical texture with reflectance values around 2% correspond to a highly aromatic material as revealed by FTIR spectroscopy with disordered internal structure consistent with moderate values of meso- and micro-porosity [61–63]. Among the woody biomasses, Pin-ca showed the lowest reflectance values, the lowest aromaticity (Table 4) and the highest volatile matter content (Table 1), all indicating a less condensed structure probably related with resinous impregnations [54]. The reflectance values (Table 5) and the volatile matter content (Table 1) of Ols-ca were similar to those of woody material, whereas its lower aromaticity (Table 4) and lower mesoporosity (Table 7) indicate a different arrangement of the chemical structure. The reflectance readings of carbonized samples had lower scatter than those of torrefied samples as indicated by the CV_{Rr} values in Table 5, indicating that increasing target temperature also increased the homogeneity of the product for a similar time of treatment.

3.4. Combustion behavior of thermally treated biomass

The torrefied samples showed similar combustion profiles to those of the raw biomasses (Fig. 4), except for their shift towards higher initial and final temperatures and the lower amount of volatiles released at low temperature. The delay in initial burning temperature (Table 6), which is essentially due to the loss of hemicellulose during torrefaction [40], resulted in a sharper burning peak for the hemicellulose/cellulose and an increase in maximum reactivity [64]. The high-temperature peak above 400 °C, essentially attributed to lignin plus the burning of resolidified carbon material, had a similar shape both in the case of the torrefied and the raw biomass samples, although the burnout temperatures in the torrefied samples were higher (Table 6). The largest differences between the biomasses could be observed in the final burning temperatures (Table 6). Ols-to was the sample with the highest final combustion temperature and, as observed in the raw samples, Pin-to had higher characteristic temperatures in the burning profiles than the hardwood samples.

In the burning profiles of the carbonized samples the peak corresponding to the decomposition of hemicellulose/cellulose completely disappeared and only one broad peak is identifiable above 300 °C (Fig. 4). This peak probably corresponded to a more refractory carbon material essentially formed by the polymerization of lignin upon carbonization with a minor contribution from the other two woody components. The maximum reactivity of this broad band was slightly higher than the peak corresponding (mostly) to lignin combustion in the raw and torrefied samples. A large displacement to higher characteristic temperatures could be observed. Differences of over to 100 °C were found between the final burning temperatures of the biochars, Euc-ca being the most reactive and Ols-ca being the least reactive. The differences observed between the burning profiles of the softwood (least reactive) and hardwood (more reactive) in the raw and torrefied samples were no longer clear after carbonization. The most significant difference was that of the final burning temperature of Ols-ca sample, which due to its more massive structure and lower mesoporosity took longer to complete combustion.

4. Conclusions

Integration of results derived from chemical, spectroscopic, physical adsorption and microscopy techniques have allowed following the transformation of softwood, hardwood and olive stone upon torrefaction and carbonization. At the torrefaction temperature used in this work (250 °C) a decrease in volatile matter and an increase of higher heating value close to 12% was achieved. These transformations, mainly due to the loss of hemicellulose, were reflected in the decrease of hydroxyl and aliphatic infrared stretching bands and a slight increase in aromaticity, which was accompanied by moderate microporosity and negligible mesoporosity development. The fluorescence intensity decreased and shifted to higher wavelengths and the reflectance increased as did the C content. Shrinkage was observed in the cell walls, resulting in a multilayered structure. Optical microscopy revealed a great heterogeneity in the samples attributed to variable time of exhibition to the target temperature due to heat diffusion from the walls to the center of the oven. The particles with thicker walls and more massive structure were more sensitive to this difference. The torrefied samples required higher temperatures to burn than the raw biomasses but their reactivities were slightly higher due to the accessibility gained with the loss of hemicellulose.

Mild carbonization at 450 °C produced an increase of around 62% of higher heating value and a decrease of 78% in volatile matter content, with a drastic loss of oxygen functionalities and a significant increase in aromaticity. The decomposition of cellulose generated a disordered carbon-rich solid with reflectance of around 1.9% and lacking fluorescence, corresponding with materials with moderate micro and meso-porosity. Biochars required higher temperatures to burn than the torrefied samples but had a higher reactivity due to the gas diffusion channels created by the mesoporosity development. At 450 °C the heat transfer effect from the walls to the center of the oven was less relevant than at 250 °C and the biochars were more homogeneous in its optical properties than the torrefied biomasses.

The slight differences observed between hardwood and softwood point towards resinous impregnation of softwood being responsible of its higher fluorescence intensity in the torrefied sample and the higher volatile matter content and the lower aromaticity remaining after mild carbonization. The differences were larger between woods and olive stone, the latter generating a more massive, less mesoporous solid, having lower aromaticity.

Acknowledgements

The financial support from a bilateral cooperation project between Brazil and Spain (CNPq 560839/2010-3; MICINN PIB2010BZ-00418) is gratefully acknowledged.

References

[1] Khorshidi Z, Ho MT, Wiley DE. The impact of biomass quality and quantity on the performance and economics of co-firing plants with and without CO_2 capture. Int J Greenhouse Gas Con 2014;21:191–202.
[2] Abbasi T, Abbasi SA. Biomass energy and the environmental impacts associated with its production and utilization. Renew Sustain Energy Rev 2010;14:919–37.
[3] Baxter L. Biomass-coal co-combustion: opportunity for affordable renewable energy. Fuel 2005;84:1295–302.
[4] Norgate T, Langberg D. Environmental and economic aspects of charcoal use in steelmaking. ISIJ Int 2009;49:587–95.
[5] Castro LA, Tavares RP. Charcoal blast furnaces process control. In: Proceedings of the iron and steel technology conference; 2004 September 15–17; Nashville, USA. Warrendale: Association for Iron & Steel Technology; 2004.
[6] Bagatini MC, Zymla V, Osório E, Vilela ACF. Characterization and reduction behavior of mill scale. ISIJ Int 2011;51:1072–9.
[7] Suopajärvi H, Pongrácz E, Fabritius T. The potential of using biomass-based reducing agents in the blast furnace: a review of thermochemical conversion technologies and assessments related to sustainability. Renew Sustain Energy Rev 2013;25:511–28.
[8] Babich A, Senk D, Fernandez M. Charcoal behaviour by its injection into the modern blast furnace. ISIJ Int 2010;50:81–8.
[9] Hanrot F, Sert D, Delinchant J, Pietruck R, Bürgler T, Babich A et al. CO_2 mitigation for steelmaking using charcoal and plastics wastes as reducing agents and secondary raw materials. In: 1st Conference on advances in materials recycling and eco-energy. Recimat09 2009, paper S05-4. <http://hdl.handle.net/10261/18433>.
[10] MacPhee JA, Gransden JF, Giroux L, Price JT. Possible CO_2 mitigation via addition charcoal to coking coal blends. Fuel Proc Technol 2009;90:16–20.
[11] Thomas S, McKnight SJ, Serrano EJ, Maslejova A, Zelinsky R, Tomás J et al. Laboratory evaluation of biomass usage for coke and sinter production. In: METEC, InSteel 2011, Düsseldorf (Germany), paper EECR-160.
[12] Diez MA, Alvarez R, Fernández M. Biomass derived products as modifiers of the rheological properties of coking coals. Fuel 2012;96:306–13.
[13] Nogami H, Yagi J, Sampaio RS. Exergy analysis of charcoal charging operation of blast furnace. ISIJ Int 2004;44:1646–52.
[14] Helle H, Helle M, Saxén, Pettersson F. Mathematical optimization of ironmaking with biomass as auxiliary reductant in the blast furnace. ISIJ Int 2009;49:1316–24.
[15] Medic D, Darr M, Shah A, Potter B, Zimmerman J. Effects of torrefaction process parameters on biomass feedstock upgrading. Fuel 2012;91:147–54.
[16] Peng JH, Bi XT, Sokhansanj S, Lim CJ. Torrefaction and densification of different species of softwood residues. Fuel 2013;111:411–21.
[17] van der Stelt MJC, Gerhauser H, Kiel JHA, Ptasinski KJ. Biomass upgrading by torrefaction for the production of biofuels: a review. Biomass Bioenergy 2011;35:3748–62.
[18] Ciolkosz D, Wallace R. A review of torrefaction for bioenergy feedstock production. Biofuels, Bioprod Bioref 2011;5(3):317–29.
[19] Kumar M, Gupta RC, Sharma T. Effects of carbonisation conditions on the yield and chemical composition of acacia and eucalyptus wood chars. Biomass Bioenergy 1992;3:411–7.
[20] Bergman PCA. Combined torrefaction and pelletisation: the TOP process. Report ECN-C-05-073. Petten, The Netherlands: ECN; 2005.
[21] Felfli FF, Luengo CA, Suárez JA, Beaton PA. Wood briquette torrefaction. Energy Sustain Dev 2005;9:19–22.
[22] Pimchuai A, Dutta AA, Basu P. Torrefaction of agriculture residue to enhance combustible properties. Energy Fuels 2010;24:4638–45.
[23] Ibrahim RHH, Darvell LI, Jones JM, Williams A. Physicochemical characterisation of torrefied biomass. J Anal Appl Pyrolysis 2013;103:21–30.
[24] Arias B, Pevida C, Fermoso J, Plaza MG, Rubiera F, Pis JJ. Influence of torrefaction on the grindability and reactivity of woody biomass. Fuel Process Technol 2008;89:169–75.
[25] Phanphanich M, Mani S. Impact of torrefaction on the grindability and fuel characteristics of forest biomass. Bioresour Technol 2011;102:1246–53.
[26] Shang L, Ahrenfeldt J, Holm JK, Sanadi AR, Barsberg S, Thomsen T, et al. Changes of chemical and mechanical behavior of torrefied wheat straw. Biomass Bioenergy 2012;40:63–70.
[27] Almeida G, Brito JO, Perré P. Alterations in energy properties of eucalyptus wood and bark subjected to torrefaction: the potential of mass loss as a synthetic indicator. Bioresour Technol 2010;101:9778–84.
[28] Antal Jr MJ, Gronli M. The art, science, and technology of charcoal production. Ind Eng Chem Res 2003;42:1619–40.
[29] Peláez-Samaniego MR, Garcia-Perez M, Cortez LB, Rosillo-Calle F, Mesa J. Improvements of Brazilian carbonization industry as part of the creation of a global biomass economy. Renew Sustain Energy Rev 2008;12:1063–86.
[30] Park S-W, Jang C-H, Baek K-R, Yang J-K. Torrefaction and low-temperature carbonization of wood biomass: evaluation of fuel characteristics of the products. Energy 2012;45:676–85.
[31] Bourke J, Manley-Harris M, Fushimi C, Dowaki K, Nunoura T, Antal Jr MJ. Do all carbonized charcoals have the same chemical structure? 2. A model of the chemical structure of carbonized charcoal. Ind Eng Chem Res 2007;46:5954–67.
[32] Brunauer S, Emmett P, Teller EJ. Adsorption of gases in multimolecular layers. Am Chem Soc 1938;60:309–15.
[33] Dubinin MM, Radushkevich LV. Equation of the characteristic curve of activated charcoal. Proc Acad Sci URSS 1947;55:331–5.
[34] Baranger R, Martínez L, Pittion J-L, Pouleau J. A new calibration procedure for fluorescence measurements of sedimentary organic matter. Org Geochem 1991;17(4):467–75.
[35] Alonso MJG, Borrego AG, Alvarez D, Kalkreuth W, Menendez R. Physicochemical transformations of coal particles during pyrolysis and combustion. Fuel 2001;80:1857–70.
[36] Demirbas A. Combustion characteristics of different biomass fuels. Prog Energy Comb Sci 2004;30(2):219–30.
[37] Pandey KK. A study of chemical structure of soft and hardwood and wood polymers by FTIR spectroscopy. J Appl Polym Sci 1999;71(12):1969–75.
[38] Pandey KK, Pitman AJ. FTIR studies of the changes in wood chemistry following decay by brown-rot and white-rot fungi. Int Biodeterior Biodegrad 2003;52:151–60.
[39] Guo Y, Bustin RM. FTIR spectroscopy and reflectance of modern charcoals and fungal decayed woods: implications for studies of inertinite in coals. Int J Coal Geol 1998;37:29–53.
[40] Yang H, Yan R, Chen H, Lee DH, Zheng C. Characteristics of hemicellulose, cellulose and lignin pyrolysis. Fuel 2007;86:1781–8.
[41] Gentzis T, Goodarzi F, McFarlane RA. Molecular structure of reactive coals during oxidation, carbonization and hydrogenation an infrared photoacoustic spectroscopic and optical microscopic study. Org Geochem 1992;18:249–58.
[42] Riesser B, Starsinic M, Squires E, Davis A, Painter PC. Determination of aromatic and aliphatic CH groups in coal by FT-IR. 2. Studies of coals and vitrinite concentrates. Fuel 1984;63:1253–61.
[43] Evans PA. Differentiating, "hard" from "soft" woods using Fourier transform infrared and Fourier transform Raman spectroscopy. Spectrochim Acta 1991;47A:1441–7.
[44] Rodrigues J, Faix O, Pereira H. Determination of lignin content of *Eucalyptus globules* wood using FTIR spectroscopy. Holzforsch 1998;52:46–50.
[45] Given PH, Spackman W, Painter PC, Rhoads CA, Ryan NJ, Alemanyl RJ, et al. The fate of cellulose and lignin in peats: an exploratory study of the input to coalification. Org Geochem 1984;6:399–407.
[46] Painter P, Starsinic M, Coleman M. Determination of functional groups in coal by Fourier transform interferometry. In: Ferraro JR, Basile LJ, editors. Fourier transform infrared spectroscopy: applications to chemical systems, vol. v. 4. London: Academic Press Inc; 1985. p. 169–240.

[47] Borrego AG, Blanco CG, Prado JG, Díaz C, Guillén MD. ^{1}H NMR and FTIR spectroscopic studies of bitumen and shale oil from selected Spanish oil shales. Energy Fuels 1996;10:77–84.

[48] Shafizadeh F. Review: introduction to pyrolysis of biomass. J Anal Appl Pyrolysis 1982;3:283–305.

[49] Michelsen JK, Khorasani GK. Monitoring chemical alterations of individual oil-prone macerals by means of microscopical fluorescence spectrometry combined with multivariate data analysis. Org Geochem 1990;15:179–92.

[50] Epidermis Esau K. In: anatomy of seed plants. 2nd ed. New York: John Wiley & Sons; 1977. p. 83–96.

[51] Órfão JJM, Antunes FJA, Figueiredo JL. Pyrolysis kinetics of lignocellulosic materials – three independent reactions model. Fuel 1999;78:349–58.

[52] Gronli MG, Várhegyi G, Di Blasi C. Thermogravimetric analysis and devolatilization kinetics of wood. Ind Eng Chem Res 2002;41:4201–8.

[53] Ghambari R, Anwar F, Alkarfy KM, Gilan A-H, Soari N. Valuable nutrients and functional bioactives in different parts of olive (*Olea europaea* L.) – a review. Int J Mol Sci 2012;13:3291–340.

[54] International Committee for Coal and Organic Petrology. ICCP handbook on coal petrology. 3rd ed. Paris: Ed. Technip; 1993.

[55] Sevilla M, Maciá-Agulló JA, Fuertes AB. Hydrothermal carbonization of biomass as a route for the sequestration of CO_2: chemical and structural properties of the carbonized products. Biomass Bioenergy 2011;35:3152–9.

[56] Jones JC. The BET surface areas of carbonised biomass [letter]. Fuel Process Technol 2013;106:784.

[57] Garrido J, Linares-Solano A, Martín-Martínez JM, Molina-Sabio M, Rodriguez-Reinoso F, Torregrosa R. Use of N_2 vs. CO_2 in the characterization of activated carbons. Langmuir 1987;3:76–81.

[58] Duber S, Rouzaud J-N, Clinard C, Pusz S. Microporosity and optical properties of some activated chars. Fuel Process Technol 2002;77–78:221–7.

[59] Sýkorová I, Pickel W, Christanis K, Wolf M, Taylor GH, Flores D. Classification of huminite—ICCP system 1994. Int J Coal Geol 2005;62:85–106.

[60] Biagini E, Narducci P, Tognotti L. Size and structural characterization of lignin–cellulosic fuels after the rapid devolatilization. Fuel 2008;87:177–86.

[61] Borrego AG, Garavaglia L, Kalkreuth WD. Characteristics of high heating rate biomass chars prepared under N_2 and CO_2 atmospheres. Int J Coal Geol 2009;77(3–4):409–15.

[62] Alvarez D, Borrego AG. The evolution of char surface area along pulverized fuel combustion. Energy Fuels 2007;21(2):1085–91.

[63] Alonso MJG, Borrego AG, Alvarez D, Parra JB, Menéndez R. Influence of pyrolysis temperature on char optical texture and reactivity. J Anal Appl Pyrolysis 2001;58–59:887–909.

[64] Diez MA, Borrego AG. Evaluation of CO_2-reactivity patterns in cokes from coal and woody biomass blends. Fuel 2013;113:59–68.